Thematic set:
Geological storage of CO_2, gas and energy

PG
Petroleum Geoscience

Published online June 27, 2017 https://doi.org/10.1144/petgeo2016-052 | Vol. 23 | 2017 | pp. 339–352

Application of material balance methods to CO_2 storage capacity estimation within selected depleted gas reservoirs

A. L. Clarke[1,2*], J. Imber[1], R. J. Davies[1,3], J. van Hunen[1], S. E. Daniels[4] & G. Yielding[5]

[1] Department of Earth Sciences, Durham University, Elvet Hill, Durham DH1 3LE, UK
[2] Present address: Badley Geoscience Ltd, North Beck Lane Hundleby, Spilsby, Lincolnshire PE23 5NB, UK
[3] Present address: School of Civil Engineering and Geosciences, Drummond Building, Newcastle University, Newcastle upon Tyne NE1 7RU, UK
[4] Geospatial Research Ltd, Department of Earth Sciences, Durham University, Elvet Hill, Durham DH1 3LE, UK
[5] Badley Geoscience Ltd, North Beck Lane Hundleby, Spilsby, Lincolnshire PE23 5NB, UK
A.L.C., 0000-0002-2715-0397; J.I., 0000-0001-9532-0776; S.E.D., 0000-0001-9917-899X
*Correspondence: amy@badleys.co.uk

Abstract: Depleted gas reservoirs are potential sites for CO_2 storage; therefore, it is important to evaluate their storage capacity. Historically, there have been difficulties in identifying the reservoir drive mechanism of gas reservoirs using traditional *P*/*z* plots, having direct impacts for the estimation of the original gas in place (OGIP) and dependent parameters for both theoretical and effective CO_2 storage capacity estimation. Cole plots have previously provided an alternative method of characterization, being derived from the gas material balance equation. We use production data to evaluate the reservoir drive mechanism in four depleted gas reservoirs (Hewett Lower Bunter, Hewett Upper Bunter, and North and South Morecambe) on the UK Continental Shelf. Cole plots suggest that the North Morecambe and Hewett Upper Bunter reservoirs experience moderate water drive. Accounting for cumulative water influx into these reservoirs, the OGIP decreases by up to 20% compared with estimates from *P*/*z* plots. The revised OGIP values increase recovery factors within these reservoirs; hence, geometrically based theoretical storage capacity estimates for the North Morecambe and Hewett Upper Bunter reservoirs increase by 4 and 30%, respectively. Material balance approaches yield more conservative estimates. Effective storage capacity estimates are between 64 and 86% of theoretical estimates within the depletion drive reservoirs, and are 53 – 79% within the water drive reservoirs.

Supplementary material: A more detailed description of the aquifer modelling is available at https://doi.org/10.6084/m9.figshare.c.3803770.v1

Received 1 April 2016; **revised** 31 March 2017; **accepted** 5 April 2017

Carbon dioxide capture and storage (CCS) is an important technology to mitigate the effect of CO_2 emissions on climate (Holloway 2009), with at least 22 large-scale CCS projects in operation or construction globally, capturing approximately 40 Mt of CO_2 per annum (Global CCS Institute 2015). The UK is predicted to rely upon fossil fuel combustion for energy generation for at least the next few decades (Holloway *et al.* 2006). As such, depleted gas fields on the UK Continental Shelf have been under consideration for CO_2 storage, offering a storage capacity of approximately 6100 Mt of CO_2 (Holloway 2009), substantially larger than that of depleted UK oil reservoirs. In comparison to alternative CO_2 storage sites, such as unmineable coal seams and saline aquifers, the dynamic behaviour of depleted gas reservoirs is well understood and a wealth of data exist for most reservoirs spanning their entire productive lifetimes. In particular, the UK Triassic Sherwood Sandstone Group (also known as the Bunter Sandstone Formation: Johnson *et al.* 1994) is considered for CO_2 storage, being a major sandstone unit with many of the necessary basic characteristics, including structural traps (such as anticlines), good porosity and permeability, large storage capacities, and a good lateral and vertical seal. Three of the largest depleted Triassic gas fields on the UK Continental Shelf are the Hewett gas field of the Southern North Sea, and the South and North Morecambe gas fields of the East Irish Sea Basin.

The CO_2 storage capacity of a depleted gas reservoir is dependent on the pressure and compressibility of the residual fluids (including gas and water) occupying the pore space. As such, it is necessary to establish whether a gas reservoir experiences a water drive, and, if so, attempt to quantify the volume of water influx into the reservoir throughout its productive lifetime. Usually, the *P*/*z* plot (reservoir pressure divided by the gas compressibility factor) is used to identify the reservoir drive mechanism: that is, establish whether a gas reservoir experiences a water drive (Vega & Wattenbarger 2000). However, it has been documented extensively within the literature that *P*/*z* plots are notoriously difficult to solve within water drive reservoirs (Agarwal *et al.* 1965; Bruns *et al.* 1965; Chierici *et al.* 1967; Dake 1978; Hagoort 1988; Pletcher 2002; Vega & Wattenbarger 2000). The insensitivity of the *P*/*z* plot, particularly within a water drive reservoir, can result in misinterpretation of the reservoir drive mechanism and a significant overestimation of the original gas in place (OGIP) (Vega & Wattenbarger 2000). Several published methods used to estimate CO_2 storage capacity rely on either direct estimation of the OGIP or a parameter that is dependent upon the OGIP (such as the recovery factor). Therefore, it is important to obtain a precise value for the OGIP to estimate the CO_2 storage capacity.

The aim of this study is to use production data and material balance methods to estimate the theoretical and effective CO_2 storage capacities in four depleted gas reservoirs with well-constrained production histories and contrasting drive mechanisms. The objectives are to: (1) compare the theoretical and effective storage capacity estimates predicted by different published analytical approaches (Bachu *et al.* 2007; Holloway *et al.* 2006; Tseng *et al.* 2012); (2) evaluate the impact of aquifer influx on

theoretical and effective storage capacity estimates for water drive reservoirs; and (3) identify which methods yield the most conservative theoretical storage capacity estimates for depletion and water drive reservoirs.

Specifically, we use production and pressure data from the Hewett, South Morecambe and North Morecambe gas fields to demonstrate the use of material balance methods in CO_2 storage capacity estimation. Production data are interpreted using both P/z plots and Cole plots (Cole 1969; Pletcher 2002) to establish reservoir drive mechanisms. This approach is taken due to the cumulative volume of produced water being unknown for these reservoirs across their productive lifetimes. For depletion drive reservoirs, OGIP is estimated via linear extrapolation of the trend on the P/z plot down to the x-axis ($y = 0$). For water drive reservoirs, an alternative methodology is used to model aquifer performance throughout the productive lifetime and to estimate the cumulative volume of water influx (W_e) into the reservoirs analysed. Once a reasonable estimate is obtained for W_e, the value can be used to calculate the OGIP. The OGIP estimates from depletion drive and water drive gas reservoirs can then be used to estimate both the theoretical and effective CO_2 storage capacities.

It is important to note that this paper uses published methods to analyse the data from the four reservoirs and is, therefore, bound to the limitations of those methods. Certain approaches, such as the use of the Cole plot, have been taken in the case of the water drive reservoirs (the Hewett Upper Bunter Sandstone and North Morecambe Sherwood Sandstone reservoirs) as there is a lack of water production data from them. As such, this paper represents an attempt at comparing estimates of CO_2 storage capacities using published material balance methods.

Our results for the Hewett Field (Fig. 1) have been derived from published data (e.g. Cooke-Yarborough & Smith 2003), and from historical field production and pressure datasets kindly provided by Eni Hewett Ltd, and which are already in the public domain (Clarke *et al.* 2010). Results for the Morecambe fields (Fig. 2) are derived from historical field production and pressure datasets kindly provided by Centrica. We emphasize that our results for the Hewett Field are entirely our own, and do not constitute interpretations or views of Eni Hewett Ltd or its partner, Perenco UK (Gas) Ltd. Similarly, our results for the South and North Morecambe fields are entirely our own, and do not constitute interpretations or views of Centrica.

Definition of 'storage capacity'

The theoretical CO_2 storage capacity is a maximum upper limit to a capacity estimate, which often represents the entire pore space of the storage complex, or the pore space with known displaceable resident fluids (Bachu *et al.* 2007). Alternatively, theoretical CO_2 storage capacity may be defined as the mass of CO_2 injected from abandonment pressure to initial reservoir pressure, to occupy the pore volume of gas produced (Tseng *et al.* 2012). Effective storage applies technical (geological and engineering) limitations to the theoretical storage capacity estimate (Bachu *et al.* 2007). In this study, effective storage capacity refers to the available pore space taking account of any residual hydrocarbons and cumulative water influx, assuming the overall pore volume is unchanged during gas production and CO_2 injection (Tseng *et al.* 2012).

Geological background

The Triassic Sherwood Sandstone Group is a major sandstone unit with many of the basic characteristics necessary for CO_2 storage, including structural traps (such as anticlines), good porosity and permeability, large storage capacities, and a good lateral and vertical seal provided by the overlying Mercia Mudstone Group – a proven hydrocarbon seal (Brook *et al.* 2003; Bentham 2006; Kirk 2006). Many of its structural anticlines occur at depths of at least 800 m; therefore, injected CO_2 may be stored in the supercritical phase assuming a geothermal gradient of 25°C km^{-1}.

The Hewett gas field

The Hewett gas field is the second largest UK North Sea gas field and the third largest UK gas field. It is located 16 km NE of Bacton on the Norfolk coastline, one of the most proximally situated gas fields on the UK Continental Shelf (Fig. 1). The Hewett gas field comprises three major reservoirs: the Triassic Upper and Lower Bunter Sandstone formations (also known as the Sherwood Sandstone Group: Warrington *et al.* 1980; Johnson *et al.* 1994), and the Permian Zechsteinkalk reservoir (Fig. 1). The Permian reservoir is not considered here for carbon storage due to its complex compartmentalization (Cooke-Yarborough & Smith 2003), which is poorly understood, and therefore it would be too expensive and high risk to develop (Bentham 2006).

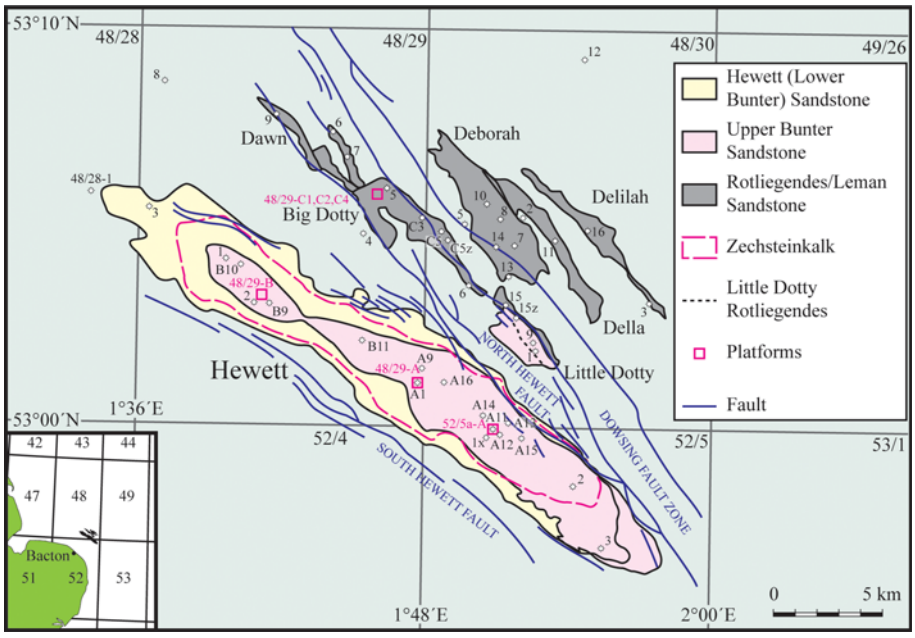

Fig. 1. Location, structure and areal extent of the gas fields of the Hewett Unit, Southern North Sea. The limit of the areal extent is defined by the original GWC within each reservoir prior to production, or fault closure of the traps. Modified from Cooke-Yarborough & Smith (2003).

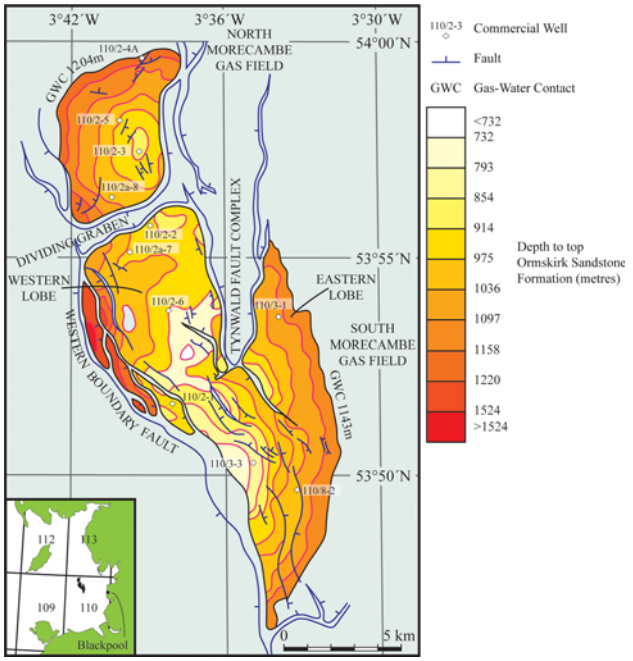

Fig. 2. Location, structure and areal extent of the South and North Morecambe gas fields of the East Irish Sea Basin. The limit of the areal extent is defined by the original GWC within each reservoir prior to production, or fault closure of the traps. Modified from Jackson *et al.* (1995).

The Hewett Upper and Lower Bunter Sandstone reservoirs define NW–SE-orientated anticlines, parallel to the original Hercynian structural trend (Fig. 1). The South Hewett Fault and Dowsing Fault Zone are reactivated Hercynian faults (Cooke-Yarborough & Smith 2003) but do not act to structurally close the Bunter reservoirs of the Hewett gas field.

The Hewett Lower Bunter structural anticline is four-way dip-closed. The Bunter Shale Formation of the Bacton Group forms the direct cap rock to the reservoir and, within the Hewett Field, maintains an almost constant thickness averaging 230 m. The stratigraphically higher Upper Bunter Sandstone structural anticline is three-way dip-closed to the north, south and west. It is closed by the North Hewett Fault on the central-eastern flank. The Dowsing Dolomitic Formation of the Haisborough Group forms the direct cap rock to the reservoir, with an average thickness of 163 m over much of the Hewett anticline, thinning towards the SE to an average of 104 m. There is greater than 600 m of overburden above the Dowsing Dolomitic Formation, consisting of the remaining formations of the Haisborough Group, the Penarth Group and the Lias Group, all of which are likely to act as secondary seals.

Production began from the Hewett Lower Bunter Sandstone reservoir in 1969, and later from the Hewett Upper Bunter Sandstone reservoir in 1973. The two reservoirs contained gas of strikingly different compositions, with the Hewett Upper Bunter reservoir containing significant quantities of hydrogen sulphide (Cooke-Yarborough & Smith 2003); evidence to suggest that the reservoirs are entirely separate from each other. Further evidence for this has been proven from production and pressure data gathered throughout their productive lifetimes, with a substantial pressure drop in the Hewett Lower Bunter Sandstone reservoir following the onset of production having no effect on the initial reservoir pressure of the Hewett Upper Bunter Sandstone reservoir (Fig. 3). The reservoirs also have different initial reservoir pressures and gas–water contacts (GWCs).

Both reservoirs consist of clean, braided fluvial and sheetflood sandstones with a high reservoir quality, although there is a degree of heterogeneity, particularly with respect to permeability. In the Hewett Lower Bunter Sandstone reservoir, the interquartile range of porosity data is between 11.8 and 24.0% with a median of 18.1%, and permeability data are between 14.5 and 1043.4 mD with a median of 195.5 mD. In the Hewett Upper Bunter Sandstone reservoir, the interquartile range of porosity data is between 15.7 and 24.2% with a median of 20.1%, and permeability data are between 43.0 and 907.5 mD with a median of 262.4 mD. Production has been straightforward in the Hewett Lower Bunter Sandstone reservoir, with a recovery factor exceeding 96% (Cooke-Yarborough & Smith 2003). The Hewett Upper Bunter has experienced recovery losses as a result of significant aquifer influx into the reservoir, but overall recovery factors are expected to exceed 90% (Cooke-Yarborough & Smith 2003). The reservoir was at risk of watering out; however, following the onset of production from the neighbouring Little Dotty Upper Bunter Sandstone reservoir, which shares the Bunter aquifer, water influx slowed substantially (Cooke-Yarborough & Smith 2003). From Figure 3, it is possible to observe a pre-production pressure drop in the Little Dotty Upper Bunter Sandstone reservoir as a result of production from the Hewett Upper Bunter Sandstone reservoir.

The Morecambe gas fields

The South Morecambe gas field is the second largest UK gas field and is located 32 miles west of Blackpool (Kirk 2006). The North Morecambe gas field is, again, of significant capacity (but smaller than South Morecambe) and is situated just to the north, separated from the South Morecambe gas field by a NE–SW-trending graben (Fig. 2). Both North and South Morecambe contain Triassic gas-producing reservoirs of the Sherwood Sandstone Group.

The South Morecambe Sherwood Sandstone reservoir is a structural anticline consisting of a northern limb, which is fault bounded to the north, west and east, and a southern limb, which is fault bounded to the west and dip-closed to the east (Stuart & Cowan 1991) (Fig. 2). The North Morecambe Sherwood Sandstone reservoir is a north–south-trending, NW-dipping fault block, fault bound to the east, west and south, but dip-closed to the north (Stuart 1993) (Fig. 2).

The South Morecambe Sherwood Sandstone reservoir has approximately 670 m of overlying sealing units (Bastin *et al.* 2003), and North Morecambe has approximately 899 m (Cowan & Boycott-Brown 2003), consisting of the Mercia Mudstone Group, the Penarth Group and the Lias Group. A narrow graben separates the South and North Morecambe gas fields. The graben's two bounding faults are considered to be full seals: the faults have substantial throws along them, meaning that the reservoirs will be juxtaposed against top seal. The reservoirs also have different reservoir pressures (Fig. 4), gas compositions and GWCs. There has been no evidence of pressure communication between the two reservoirs over their productive lifetimes (Fig. 4). North Morecambe has several small faults within the reservoir; however, the only significant internal fault has a 30 m maximum throw and defines an easterly fault terrace that is in pressure communication with the remainder of the reservoir (Cowan & Boycott-Brown 2003).

Both reservoirs consist of fluvial (braided stream and sheetflood) sandstones (Stuart & Cowan 1991). The main control on reservoir properties and performance is governed by authigenic platy illite abundance and distribution. Platy illite was originally precipitated beneath a palaeo-GWC (Bastin *et al.* 2003). In the illite-free zone, the reservoirs enjoy relatively good reservoir properties with reasonably high porosity and permeability values despite a degree of heterogeneity. However, in the illite-affected zone, permeability can be reduced by up to two orders of magnitude (Stuart 1993).

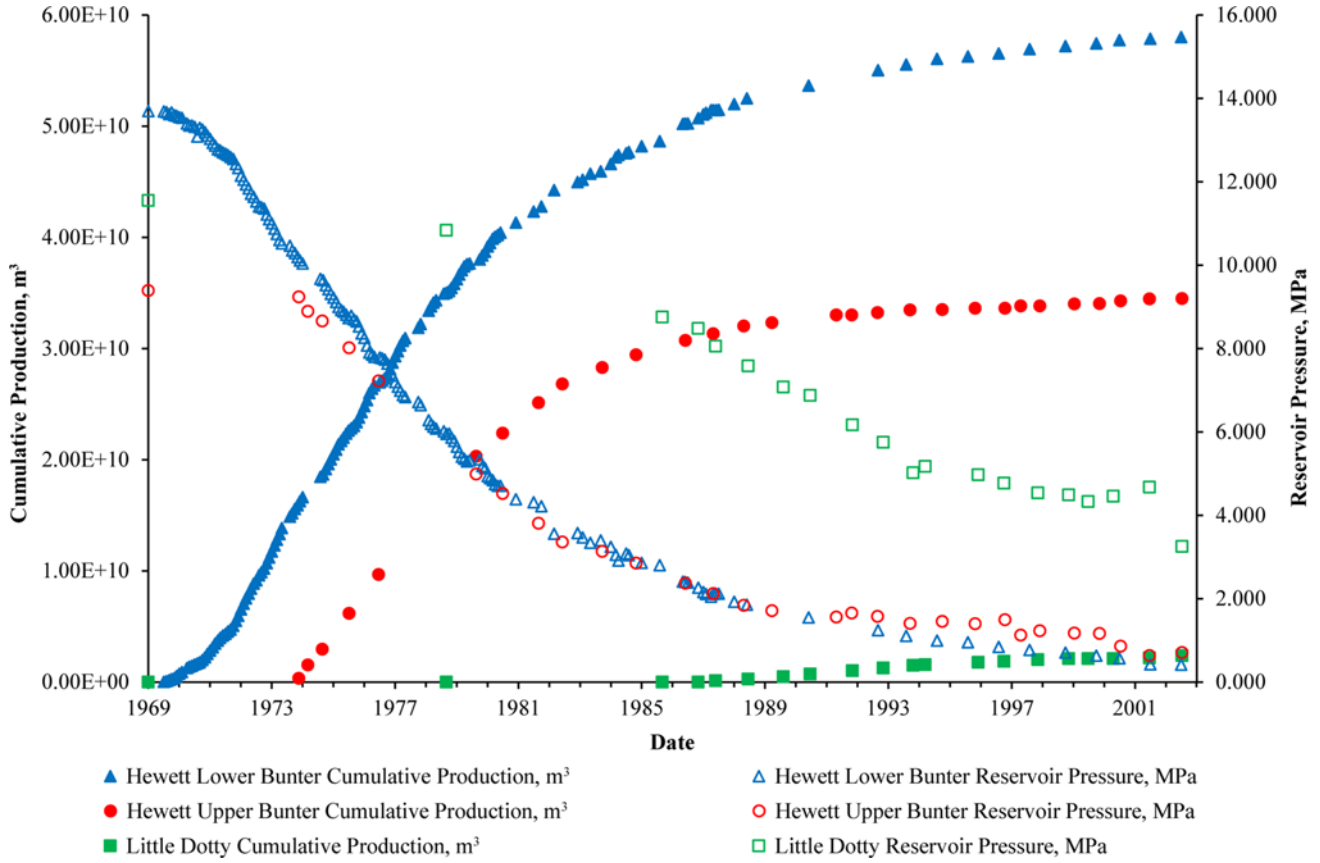

Fig. 3. Production and pressure data for the Hewett Upper and Lower Bunter Sandstone reservoirs and the Little Dotty Upper Bunter Sandstone reservoir. The dashed lines indicate the dates when the reservoirs came online.

In the illite-free zone of the South Morecambe Sherwood Sandstone reservoir, the interquartile range of porosity data is between 7.8 and 14.3% with a median of 10.8%, and permeability data are between 0.3 and 28.9 mD with a median of 2.8 mD. In the illite-affected zone, interquartile range of porosity data is between 10.7 and 16.5% with a median of 13.6%, and permeability data are between 0.2 and 8.5 mD with a median of 1.2 mD.

Likewise, in the illite-free zone of the North Morecambe Sherwood Sandstone reservoir, the interquartile range of porosity data is between 11.6 and 17.7% with a median of 14.7%, and permeability data are between 6.5 and 287.5 mD with a median of 64.0 mD. In the illite-affected zone, the interquartile range of porosity data is between 7.5 and 13.0% with a median of 10.0%, and permeability data are between 0.05 and 2.2 mD with a median of 0.3 mD – greatly reduced due to the presence of illite.

Despite this, production from the illite-free zone has been successful, with recovery factors of 93% in South Morecambe and 80% in North Morecambe.

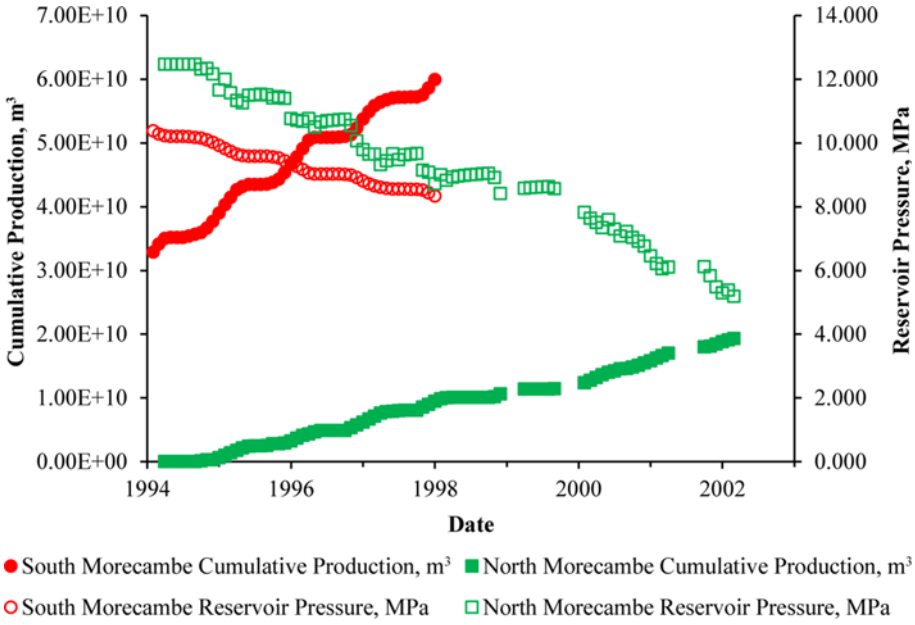

Fig. 4. Production and pressure data for the North Morecambe and South Morecambe Sherwood Sandstone reservoirs.

Distinguishing reservoir drive mechanism and estimating the OGIP

Material balance, or the P/z plot, is a popular method used to establish the presence (or absence) of a water drive within producing gas reservoirs and to estimate the OGIP (Agarwal *et al.* 1965; Bruns *et al.* 1965; Chierici *et al.* 1967; Dake 1978; Archer & Wall 1986; Hagoort 1988; Vega & Wattenbarger 2000; Pletcher 2002). The material balance equation is particularly suited to true depletion drive (volumetric) reservoirs: that is, reservoirs that experience no water encroachment throughout their productive lifetime and no reservoir compaction. As such, the initial gas volume at the initial reservoir pressure is equal to the remaining gas volume at lower pressure (Archer & Wall 1986). Hence:

$$G(B_{gi}) = (G - G_p)B_g \tag{1}$$

where G is the original gas in place, B_g is the gas formation volume factor (reservoir volume/standard condition volume), G_p is the cumulative volume of produced gas and the subscript, i, denotes the initial reservoir conditions (after Archer & Wall 1986).

The gas formation volume factor (B_g) is a ratio between reservoir and standard condition volumes. Therefore, the real gas equation of state ($PV = znRT$) can be substituted, where P is the reservoir pressure, V is the gas volume, z is the gas compressibility factor, n is the number of moles of gas, R is the gas constant and T is the reservoir temperature. In an isothermal reservoir (where the initial reservoir temperature is equal to the current reservoir temperature), the equation can be expressed in linear form (after Archer & Wall 1986):

$$\frac{P}{z} = \left(-\frac{P_i}{z_i G}\right)G_p + \frac{P_i}{z_i} \tag{2}$$

In a true depletion drive reservoir, the cumulative volume of produced gas (G_p) will be equal to the OGIP at $P/z = 0$. Therefore, linear extrapolation of production data on the P/z plot to the x-axis ($P/z = 0$) provides a reliable estimate of OGIP (see Fig. 5). Likewise, any estimates of theoretical mass CO_2 storage capacity (an estimate of the maximum volume of CO_2 that can be stored within a site: Bachu *et al.* 2007) based on this method should also yield reliable results.

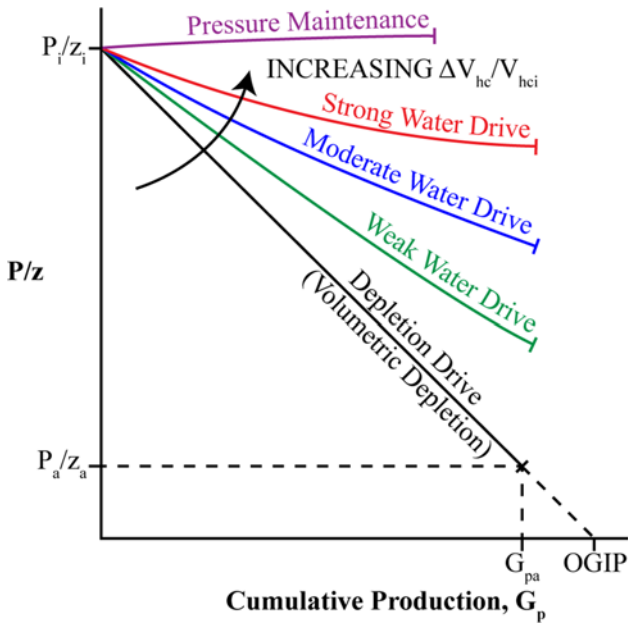

Fig. 5. Material balance (P/z) plot showing major trends depending on the degree of aquifer influx into a reservoir assuming all pressure support to the producing reservoir is a result of aquifer influx. Modified from Hagoort (1988).

However, difficulties arise in solving the material balance equation in the presence of a water drive. The majority of gas reservoirs experience some degree of water drive: production typically induces aquifer influx to the reservoir. The reduction in reservoir pressure (as production progresses) leads to an expansion of aquifer water that results in aquifer (water) influx into the pore space liberated (Dake 1978). The proportion of liberated pore space occupied by water is dependent on the rate of aquifer influx, or aquifer strength. The cumulative volume of water influx at reservoir conditions (W_e) is an important parameter within water drive reservoirs. It gives an indication of aquifer strength and governs the reservoir performance whilst providing a degree of pressure support to the gas reservoir (see Fig. 5). On a P/z plot, field data will typically deviate from linearity as a result of aquifer influx (increasing pressure support and W_e) or aquifer depletion (decreasing pressure support and W_e by fluid transport to another reservoir). As such, the material balance equation (after Archer & Wall 1986) becomes:

$$G(B_{gi}) = (G - G_p)B_g + W_e - W_pB_w \tag{3}$$

where W_p is the cumulative volume of produced water and B_w is the water formation volume factor.

Equation (3) can be rearranged as:

$$\frac{G_pB_g}{B_g - B_{gi}} = G + \frac{W_e - W_pB_w}{B_g - B_{gi}} \tag{4}$$

Consequently, identification of the reservoir drive mechanism on a P/z plot can be ambiguous (Vega & Wattenbarger 2000), particularly at the beginning of the productive lifetime of the reservoir when there is only a small amount of production data available. Despite water drive reservoirs showing a slightly curved trend across their entire lifetimes in Figure 5, they could easily be interpreted to be linear in the initial stages of production, leading to misidentification of the reservoir drive mechanism (i.e. depletion drive rather than water drive). In such cases, linear extrapolation of data points on the P/z plot will give erroneously high values of OGIP and, hence, will have implications for the CO_2 storage capacity estimation (see Fig. 5).

Data from the four case study reservoirs are presented on P/z plots in Figure 6. The gas pressure–volume–temperature (PVT) properties, here and elsewhere in the study, were estimated using the Peng–Robinson equation of state (Peng & Robinson 1976), as it allows for accurate estimation of fluid properties specifically within natural gas reservoirs. The estimated reservoir volumes vary due to the varying reservoir pressures, which could be well constrained from the regular measurements, and the temperature which was measured only initially and was therefore kept constant in the absence of more recent data. In all four cases, data appear to confirm a linear trend, with some reservoirs showing a small amount of fluctuation about the trend. As such, the reservoir drive mechanism of all four reservoirs was originally considered to be depletion drive, and linear extrapolation of the datasets to the x-axis provides an estimation of the OGIP (Table 1). This initial interpretation is now checked by re-plotting the same data on a Cole plot (Pletcher 2002).

The use of cole plots to distinguish drive mechanism within a gas reservoir and to estimate aquifer strength

The Cole plot (Cole 1969) enables a clear distinction between depletion and water drive reservoirs (Pletcher 2002): depletion drive reservoirs display a positive linear trend, whereas water drive reservoirs show a curve, and the shape of the curve provides a qualitative assessment of the strength of the water drive (weak, moderate or strong) (see Fig. 7). As such, a water drive reservoir is clearly distinguishable from a depletion drive reservoir early in its productive lifetime. It assumes that the expansibility of water is small compared to that of gas and, as such, is highly sensitive to the effects

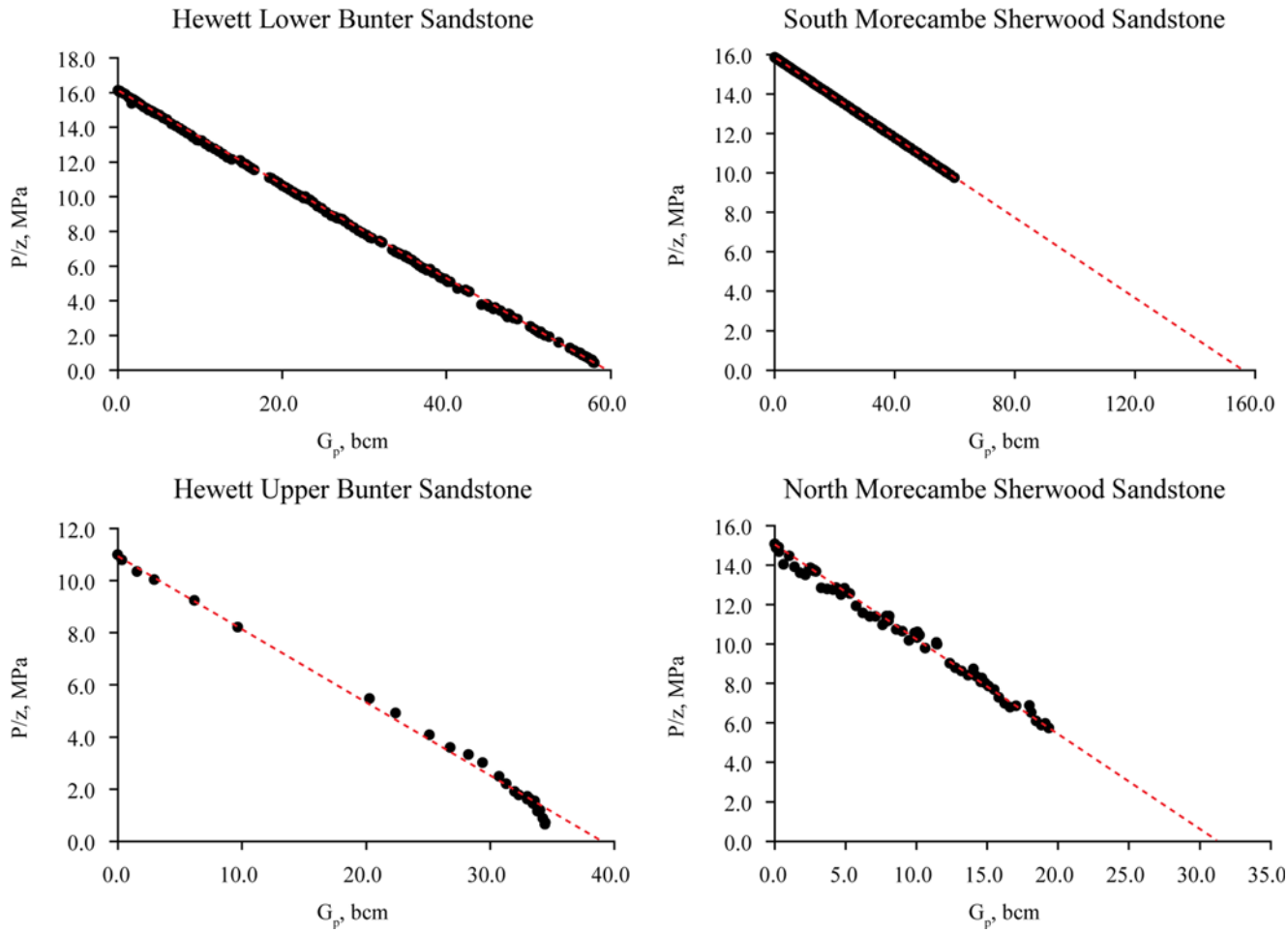

Fig. 6. *P*/*z* plots of the four reservoirs: Hewett Lower Bunter Sandstone, Hewett Upper Bunter Sandstone, South Morecambe Sherwood Sandstone and North Morecambe Sherwood Sandstone. All four reservoirs have been interpreted as having a depletion drive reservoir mechanism based on the linear trends of the plots indicated by the red dashed lines. Please note: results for the Hewett reservoirs do not constitute an Eni interpretation or view.

of water influx making it a good qualitative tool. However, it may not be possible to identify aquifer strength until later in the productive lifetime as the overall shape of the curve needs to be observed. This approach to estimate aquifer strength within the water drive reservoirs (and therefore the cumulative volume of water influx, W_e) has been used in the absence of water production data from them.

The Cole plot (Cole 1969) involves plotting the left-hand side of equation (4), $G_pB_g/(B_g - B_{gi})$ (the cumulative volume of gas produced at standard conditions multiplied by the gas formation volume factor divided by the difference between the current and initial gas formation volume factor), on the *y*-axis v. the cumulative volume of gas produced, G_p, on the *x*-axis. For depletion drive reservoirs, the term on the far right-hand side of equation (4), $(W_e - W_pB_w)/(B_g - B_{gi})$ (the cumulative volume of water influx minus the cumulative volume of water produced at the wells multiplied by the water formation volume factor, divided by the difference between the current and initial gas formation volume factor), goes to zero and the points plot linearly with the *y*-intercept equal to *G* (the OGIP). However, within water drive reservoirs, this term is no longer equal to zero and points plot with a curved trend.

Where a weak water drive is present, $(W_e - W_pB_w)/(B_g - B_{gi})$ decreases with time as the denominator (gas expansion) increases faster than the numerator (net water influx); therefore, the resulting plot will have a negative slope that progresses towards the OGIP as

Table 1. *Estimates of original gas in place based on Cooke-Yarborough & Smith (2003) for the Hewett reservoirs, and extrapolation of a linear trend on P/z plots of reservoir data for the South Morecambe and North Morecambe gas fields (shown in Fig. 4)*

Reservoir	OGIP (bcm)
Hewett Lower Bunter Sandstone	59.5
Hewett Upper Bunter Sandstone	38.4
South Morecambe Sherwood Sandstone	155.7
North Morecambe Sherwood Sandstone	36.5

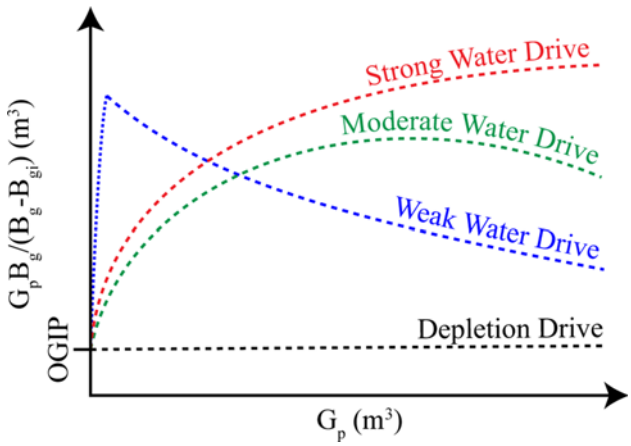

Fig. 7. Major trends on a Cole plot. Cole plots can provide a clearer distinction between water drive and depletion drive reservoirs than a *P*/*z* plot as any degree of water influx into a reservoir produces a curve on the Cole plot. The overall shape of the curve indicates aquifer strength. Redrawn from Pletcher (2002).

production continues (Wang & Teasdale 1987). For moderate and strong water drive, the shape of the curve on the Cole plot is dependent on the gas formation volume factor, which, in turn, is dependent on both the cumulative volume of water influx, W_e, and the cumulative volume of produced gas, G_p. In both cases, initially the rate of $G_pB_g/(B_g - B_{gi})$ increases at a decreasing rate. In reservoirs with a strong water drive, this is maintained throughout the productive lifetime, resulting in a concave-down increasing curve. However, in reservoirs with a moderate water drive, when the volume of produced hydrocarbons is nearing the volume of the OGIP, $G_pB_g/(B_g - B_{gi})$ begins to decrease at an increasing rate, resulting in a concave-down curve on the Cole plot across the entire productive lifetime.

When data from the Hewett Lower Bunter Sandstone reservoir and South Morecambe Sherwood Sandstone reservoir are plotted on a Cole plot, they conform well to an overall linear trend (Fig. 8). Hence, the reservoir drive mechanism is confirmed as depletion drive. The scatter observed on the plot shortly after the onset of production can probably be explained by small errors in pressure measurement (Pletcher 2002). If a pressure gradient existed in the reservoir, wells in different areas will record different pressures under reasonable shut-in times (Payne 1996). Pressure can also be influenced by a well's previous production rate (Payne 1996). This often occurs following the onset of production until the reservoir matures and the production rate stabilizes.

However, when data from the Hewett Upper Bunter Sandstone reservoir and North Morecambe Sandstone reservoir are plotted on a Cole plot, a curved trend is observed that suggests the reservoirs experience a degree of water drive (Fig. 8). Data from the Hewett Upper Bunter Sandstone reservoir show that towards the end of the productive lifetime, the curve on the Cole plot appears to decrease; therefore, it is possible to characterize the reservoir drive mechanism as moderate water drive. This is consistent with a water influx ranging between 15 and 50% of the reservoir volume (Hagoort 1988), and is also consistent with the observations of Cooke-Yarborough & Smith (2003) with respect to the reservoir experiencing significant water influx from the Bunter aquifer. Please note: results for the Hewett Upper Bunter Sandstone reservoir does not constitute an Eni interpretation or view.

Data from the North Morecambe Sherwood Sandstone reservoir fluctuate about the curved trend (Fig. 8). This is partially due to seasonal production from the reservoir. Hence, identification of aquifer strength is not definitive: the reservoir is most likely to have a moderate to strong water drive. As the reservoir is not fully depleted at the limit of the data shown here, it is not possible to observe the presence or absence of the tail-off in the trend which could identify the aquifer strength.

Quantifying the volume of water influx into a gas reservoir

Due to the Hewett Upper Bunter Sandstone reservoir and the North Morecambe Sherwood Sandstone reservoir datasets showing the presence of a water drive when plotted on a Cole plot, it is likely that the OGIP estimated from the P/z plot is an overestimate, as it

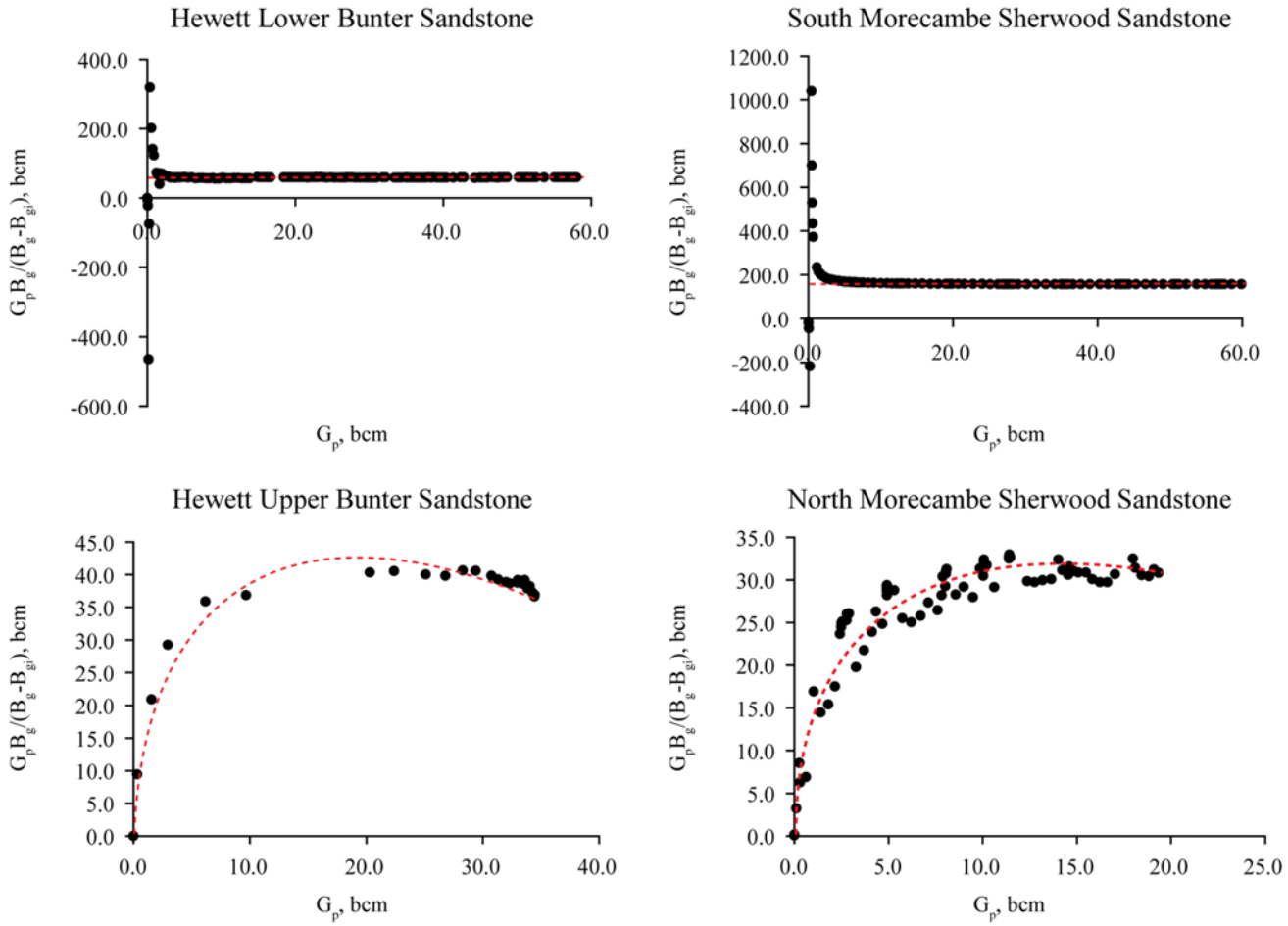

Fig. 8. Cole plots of the four reservoirs: Hewett Lower Bunter Sandstone, Hewett Upper Bunter Sandstone, South Morecambe Sherwood Sandstone and North Morecambe Sherwood Sandstone. The Hewett Lower Bunter Sandstone and South Morecambe Sherwood Sandstone reservoirs have been confirmed to have a depletion drive reservoir mechanism, whereas the Hewett Upper Bunter Sandstone and North Morecambe Sherwood Sandstone reservoirs show a moderate water drive mechanism when their data are plotted on the Cole plot. Please note: results for the Hewett reservoirs do not constitute an Eni interpretation or view.

Table 2. *(a) Estimates of W_e based on the original estimated values for OGIP for the Hewett Upper Bunter Sandstone (Cooke-Yarborough & Smith 2003) and North Morecambe Sherwood Sandstone (P/z plots in Fig. 4), assuming they are depletion drive reservoirs, using equation (1). (b) Estimates of OGIP using equation (10, based on mean W_e values (cumulative volume of water influx into a reservoir) from aquifer models*

		Hewett Upper Bunter		North Morecambe	
		W_e (m^3)	OGIP (m^3)	W_e (m^3)	OGIP (m^3)
(a)	Estimated W_e based on industry estimate OGIP	-2.153×10^8	3.840×10^{10}	-6.745×10^7	3.653×10^{10}
(b)	Finite radial aquifer mean	1.700×10^7	3.680×10^{10}	1.820×10^7	2.927×10^{10}
	Finite linear aquifer mean	4.190×10^6	3.689×10^{10}	1.560×10^7	2.949×10^{10}
	Mean of radial and linear models	1.060×10^7	3.685×10^{10}	1.690×10^7	2.938×10^{10}

Please note: results for the Hewett Upper Bunter Sandstone reservoir do not constitute an Eni interpretation or view.

assumes the reservoir experiences depletion drive only. To check this estimate, equation (5) (after Dake 1978) can be used to estimate a value for the cumulative volume of water influx into a reservoir, W_e, in the absence of water production data from the two reservoirs:

$$W_e = \frac{G_p - \mathrm{OGIP}\,(1 - E/E_i)}{E} \tag{5}$$

where G_p is the cumulative volume of produced hydrocarbons, E is the gas expansion factor (the reciprocal of the gas formation volume factor, B_g) and the subscript, i, denotes initial reservoir conditions.

Within a depletion drive gas reservoir, the value of W_e will be zero, or close to it, as there is little or no water encroachment throughout production. However, if a water drive reservoir has been misidentified as a depletion drive reservoir, then the OGIP may have been overestimated, which would result in an incorrect (negative) value for W_e. Table 2(*a*) shows the estimated values of W_e estimated using equation (5) for the Hewett Upper Bunter Sandstone reservoir and the North Morecambe Sherwood Sandstone reservoir. In both reservoirs, the estimated value of W_e is negative, and therefore there is further evidence to suggest that the OGIP values estimated originally from the *P*/*z* plots are incorrect. If both reservoirs experience a water drive as indicated by their respective Cole Plots, their estimated W_e values should be positive: that is, they should experience aquifer influx as gas is produced from them.

Aquifer models can be used to estimate W_e, from which a range of OGIP can be estimated. This revised OGIP estimates can then be input into CO_2 storage capacity equations to give a more accurate estimate of the CO_2 storage capacity. In this study, the unsteady state water influx theory of Van Everdingen & Hurst (1949) was used to estimate the cumulative volume of water influx throughout the productive lifetimes of the Hewett Upper Bunter Sandstone and North Morecambe Sherwood Sandstone reservoirs.

Aquifers can be classified as radial or linear. The Hewett and Morecambe gas fields share characteristics with both radial and linear aquifer types due to their trap geometries; therefore, both radial and linear models were evaluated. Equation (6) can be used to estimate W_e for both a radial aquifer and a linear aquifer:

$$W_e = U \Delta P W_D(t_D) \tag{6}$$

where U is the aquifer constant, ΔP is the pressure change over the time interval being assessed and $W_D(t_D)$ is the dimensionless cumulative water influx function (after Dake 1978).

Estimation of the aquifer constant, U, differs for radial and linear aquifers, and is described fully in Dake (1978). Radial aquifers rely upon the estimation of the encroachment angle, f, using equation (7) for aquifers that subtend angles of less than 360°, and which can be estimated from the reservoir geometry (see Fig. 9a). The Hewett Upper Bunter Sandstone reservoir is fault bounded to the east by the North Hewett Fault and the South Hewett Fault also runs parallel to the western flank of the anticline, although it is thought not to close the reservoir. This implies flow can occur in a NW–SE orientation (see Fig. 9b). The North Morecambe Sherwood Sandstone reservoir is fault bounded to the east, south and west; therefore, the angle of water encroachment into the reservoir is estimated to be 90° from the north (see Fig. 9c):°

$$f = \frac{(\text{encroachment angle})^\circ}{360^\circ} \tag{7}$$

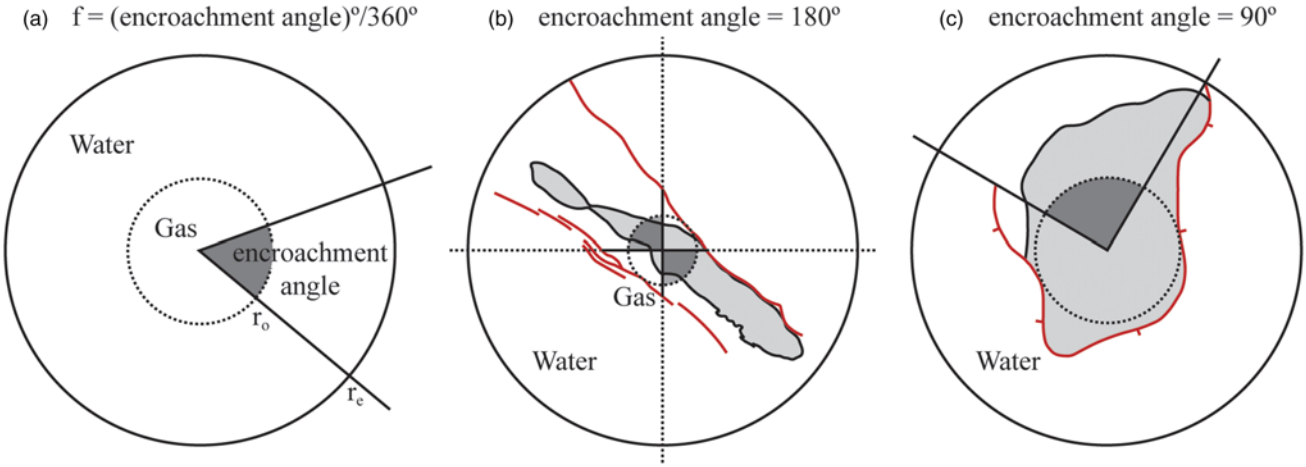

Fig. 9. Radial aquifer geometry: (**a**) schematic, redrawn from Dake (1978); (**b**) the Hewett Upper Bunter Sandstone reservoir; and (**c**) the North Morecambe Sherwood Sandstone reservoir. The reservoir outlines in (b & c) can be observed with the bounding faults in red. In (b) the encroachment angle is 180° with water influx from both the NW and the SE. In (c) the encroachment angle is 90° with water influx from the north. Please note: results for the Hewett Upper Bunter Sandstone reservoir does not constitute an Eni interpretation or view.

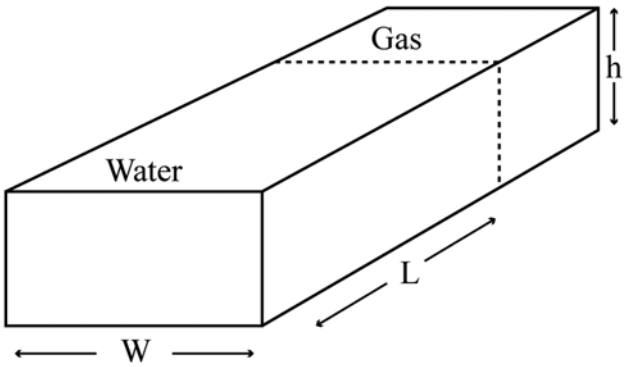

Fig. 10. Linear aquifer geometry schematic, redrawn from Dake (1978).

For linear aquifers, estimation of the aquifer constant, U, is more simple, requiring the width and length of the aquifer (see Fig. 10). Aquifer length, estimated from the hydraulic diffusivity, κ_ϕ (after Wibberley 2002), was used to evaluate an order-of-magnitude estimate for the characteristic diffusion distance for a pressure pulse within the water leg to diffuse over a specified time, based on the pressure depletion history (Figs 2 and 4), permeability and porosity data for the reservoirs:

$$\kappa_\phi = \frac{k}{\mu\phi\,(c_{\text{res}} + c_{\text{fluid}})} \tag{8}$$

$$\Delta x = \sqrt{(\kappa_\phi\,\Delta t)} \tag{9}$$

where k is the permeability, μ is the viscosity, ϕ is the porosity, c_{res} is the bulk compressibility of the matrix, c_{fluid} is the bulk compressibility of the fluid, Δx is the characteristic diffusion distance and Δt is the characteristic diffusion time.

As described previously, a host of porosity and permeability data has been gathered from multiple wells across the reservoirs which showed a considerable amount of variability. Conversely, the viscosity and the bulk compressibility of the reservoirs and fluids could be better constrained. As such, Monte Carlo simulation was used to estimate the hydraulic diffusivity. This analyses risk for any parameter displaying natural uncertainty through the use of a probability distribution.

The results gave a hydraulic diffusivity of 0.026 $m^2\ s^{-1}$ in the Hewett Upper Bunter Sandstone reservoir and 0.012 $m^2\ s^{-1}$ in the North Morecambe Sherwood Sandstone reservoir, with an estimated aquifer length of 5.73 and 1.76 km, respectively.

Using the estimates of W_e obtained using the finite radial and linear aquifer models, it is possible to obtain values of OGIP for both case study reservoirs through rearranging equation (5):

$$\text{OGIP} = \frac{G_p - W_e E}{1 - E/E_i}. \tag{10}$$

Results are shown in Table 2(*b*), along with the mean W_e values of the radial and linear aquifer models. It can be seen that OGIP estimates are reduced by a maximum of 1.60 bcm (billion cubic metres) of natural gas in the Hewett Upper Bunter Sandstone reservoir (4.2%), and by a maximum of 7.26 bcm of natural gas in the North Morecambe Sherwood Sandstone reservoir (19.9%). As such, this analysis suggests that the OGIP values originally estimated from the P/z plots for both reservoirs are too large, which can impact CO_2 storage capacity estimates. Please note: results for the Hewett Upper Bunter Sandstone reservoir does not constitute an Eni interpretation or view.

Importance of theoretical mass CO_2 storage capacity estimation

Four published theoretical CO_2 storage capacity equations and one effective CO_2 storage capacity equation have been used in this study (Table 3; see Table 4 for the nomenclature used). There are two main approaches to estimating the theoretical CO_2 storage capacity of depleted gas reservoirs. The first approach adapts the geometrically based STOIIP (stock tank oil initially in place) method, used frequently in the oil and gas industry to estimate the volume of reserves: for example, the method of Bachu *et al.* (2007) (Table 3, equation 1). The second approach is based on the principle that a variable proportion of the pore space occupied by the recoverable reserves will be available for CO_2 storage: for example, the methods of Holloway *et al.* (2006), Bachu *et al.* (2007) and Tseng *et al.* (2012) (Table 3, equations 2, 3 and 4, respectively).

The effective CO_2 storage capacities of the case study reservoirs were estimated using the method of Tseng *et al.* (2012) (Table 3, equations 5 and 6). This provides an analytical method for estimation based on material balance and uses parameters that are generally well constrained within depleted gas reservoirs, whether they be depletion drive or water drive reservoirs. Unfortunately, the effective CO_2 storage capacities of the case study reservoirs could not be estimated using the equation of Bachu *et al.* (2007) (Table 3, equation 7). The method relies upon knowledge of capacity coefficients that are difficult to constrain, there are few published studies that calculate them and there are no data specifically relating to CO_2 storage in depleted gas reservoirs.

Table 3. *Published theoretical and effective CO_2 storage capacity equations for depleted gas reservoirs*

Storage capacity equation	Reference	Equation number
Theoretical CO_2 storage capacity equations:		
$M_{CO_2t} = \rho_{CO_2r}[R_f A h \varphi(1 - S_w) - V_{iw} + V_{pw}]$	Bachu *et al.* (2007)	1
$M_{CO_2t} = \rho_{CO_2r} R_f (1 - F_{IG})\,\text{OGIP}\left\lfloor\frac{(P_s Z_r T_r)}{(P_r Z_s T_s)}\right\rfloor$	Bachu *et al.* (2007)	2
$M_{CO_2t} = \left(\frac{V_{GAS}[stp]}{B_{igas}}\,\rho_{CO_2r}\right)$	Holloway *et al.* (2006)	3
$M_{CO_2t} = \frac{\rho_{CO_2r}(G_{phc}\,B_{gas})}{B_{iCO_2}} = \frac{\rho_{CO_2r}(G_{phc}\,z_{gas})}{z_{iCO_2}}$	Tseng *et al.* (2012)	4
Effective CO_2 storage capacity equations:		
$M_{injCO_2} = \rho_{CO_2r}\,G_{injCO_2}$	Tseng *et al.* (2012)	5
where		
$G_{injCO_2} = G_{phc} - G_{ihc} + \frac{P_{reshc/CO_2}}{z_{reshc/CO_2}}\left(\frac{z_{ihc}}{P_{ihc}}G_{ihc} - W_e\frac{T_{sc}}{P_{sc}T}\right)$	Tseng *et al.* (2012)	6
$M_{CO_2e} = C_m C_b C_h C_w C_a M_{CO_2t} \equiv C_e M_{CO_2t}$	Bachu *et al.* (2007)	7

See Table 4 for an explanation of parameters.

Table 4. *Nomenclature used for the theoretical and effective storage capacity equations in Table 3*

Abbreviation	Definition	Units
ϕ	Reservoir porosity	Dimensionless
ρ_{CO_2r}	Density of carbon dioxide at reservoir conditions	kg m^{-3}
A	Reservoir/play area	m^2
B_{gas}	Reservoir gas formation volume factor at end of production	Dimensionless
B_{iCO_2}	CO_2 formation volume factor at initial reservoir conditions	Dimensionless
B_{igas}	Gas formation volume factor at initial reservoir conditions	Dimensionless
C_a	Capacity coefficient for aquifer strength	Dimensionless
C_b	Capacity coefficient for buoyancy	Dimensionless
C_e	Effective capacity coefficient	Dimensionless
C_h	Capacity coefficient for heterogeneity	Dimensionless
C_m	Capacity coefficient for mobility	Dimensionless
C_w	Capacity coefficient for water saturation	Dimensionless
E	Gas expansion factor	Dimensionless
F_{IG}	Fraction of injected gas	Dimensionless
G_{ihc}	Volume of initial hydrocarbons	m^3
G_{injCO_2}	Cumulative volume of injected CO_2	m^3
G_{phc}	Volume of produced hydrocarbons	m^3
h	Reservoir height/thickness	m
M_{CO_2e}	Effective mass storage capacity for CO_2	tonnes
M_{CO_2t}	Theoretical mass storage capacity for CO_2	tonnes
M_{injCO_2}	Effective mass storage capacity for injected CO_2	tonnes
OGIP	Original gas in place	m^3
P_{ihc}	Pressure at initial reservoir conditions	Pa
P_r	Reservoir pressure	Pa
P_{reshc/CO_2}	Pressure of residual hydrocarbon/CO_2 mix	Pa
P_s	Surface pressure	Pa
P_{sc}	Pressure at standard conditions	Pa
R_f	Recovery factor	Dimensionless
S_w	Water saturation	Dimensionless
T	Reservoir temperature	Kelvin
T_r	Reservoir temperature	Kelvin
T_s	Surface temperature	Kelvin
T_{sc}	Temperature at standard conditions	Kelvin
V_{GAS}	Volume of ultimate recoverable reserves	m^3
V_{iw}	Volume of injected water	m^3
V_{pw}	Volume of produced water	m^3
W_e	Cumulative volume of water influx into a reservoir	m^3
z_{gas}	Reservoir gas compressibility factor at end of production	Dimensionless
z_{iCO_2}	CO_2 gas compressibility factor at initial reservoir conditions	Dimensionless
z_{ihc}	Gas compressibility factor at initial reservoir conditions	Dimensionless
z_{reshc/CO_2}	Gas compressibility factor of residual hydrocarbon/CO_2 mix	Dimensionless
Z_r	Reservoir compressibility	Dimensionless
Z_s	Surface compressibility	Dimensionless

When estimating both theoretical and effective CO_2 storage capacity, CO_2 density and the gas compressibility factor have been estimated using the Peng–Robinson equation of state (Peng & Robinson 1976), along with the modelling tool, RefProp (Lemmon *et al.* 2013). The results were modelled using the specific natural gas composition of the individual reservoirs, and therefore produce well-constrained results being governed by the temperature and pressure of the reservoir.

The gas formation volume factor, B_g, is used to relate the volume of a fluid phase existing at reservoirs conditions of temperature and pressure to its equivalent volume at standard conditions (Archer & Wall 1986). It is equal to the reservoir volume divided by the standard condition volume and relies upon estimation of the gas compressibility factor, and, as such, produces well-constrained results.

Table 5 and Figure 11 show the estimated theoretical CO_2 storage capacities of the four reservoirs calculated using the original estimated values for OGIP. The water drive reservoirs (Hewett Upper Bunter and North Morecambe Sherwood Sandstone) have additional results based on the W_e and OGIP estimates from the radial and linear aquifer modelling, and also an average of the two models. From Table 5, theoretical estimates vary by 16% in the Hewett Lower Bunter reservoir, 81% in the Hewett Upper Bunter reservoir, 88% in the South Morecambe reservoir and 91% in the North Morecambe reservoir (percentage difference between the highest and lowest estimates, based on average aquifer models in the water drive reservoirs).

It can be seen from the results using the geometric method of Bachu *et al.* (2007) (Table 3, equation 1), the theoretical CO_2 storage capacities of the water drive reservoirs are increased when the OGIP is estimated via aquifer modelling. This is even more apparent in Figure 12, which shows the percentage difference between the theoretical CO_2 storage capacity estimates in the water drive reservoirs compared to those estimated originally, represented by the dashed line (zero difference). Figure 12 shows that originally the storage capacities may have been underestimated using original OGIPs by approximately 4% in the Hewett Upper Bunter Sandstone reservoir, and approximately 30% in the North Morecambe Sherwood Sandstone reservoir using the geometric method of

Table 5. *Estimated theoretical mass CO_2 storage capacities of the four reservoirs*

	Depletion drive reservoirs		Water drive reservoirs	
	Hewett Lower Bunter	South Morecambe	Hewett Upper Bunter	North Morecambe
Tseng *et al*. (2012)				
Industry	2.81×10^8	3.26×10^8	1.78×10^8	1.55×10^8
Radial			1.78×10^8	1.55×10^8
Linear			1.78×10^8	1.55×10^8
Average			1.78×10^8	1.55×10^8
Bachu *et al*. (2007, equation 1)				
Industry	2.49×10^8	2.53×10^8	7.94×10^8	8.20×10^8
Radial			8.27×10^8	1.07×10^9
Linear			8.26×10^8	1.06×10^9
Average			8.26×10^8	1.07×10^9
Bachu *et al*. (2007, equation 2)				
Industry	2.43×10^8	3.12×10^8	1.55×10^8	1.03×10^8
Radial			1.55×10^8	1.03×10^8
Linear			1.55×10^8	1.03×10^8
Average			1.55×10^8	1.03×10^8
Holloway *et al*. (2006)				
Industry	2.35×10^8	3.07×10^8	1.57×10^8	1.00×10^8
Radial			1.57×10^8	9.99×10^7
Linear			1.57×10^8	9.99×10^7
Average			1.57×10^8	9.99×10^7

All reservoir capacities have been calculated using the original estimated values for OGIP. The two water drive reservoirs (Hewett Upper Bunter Sandstone and North Morecambe Sherwood Sandstone) also have estimates based on radial and linear aquifer modelling, and an average of the two models. Please note: results for the Hewett reservoirs do not constitute an Eni interpretation or view.

Bachu *et al*. (2007). It is also only this equation that is susceptible to variation as a result of the aquifer modelling, as can be seen in Figure 12. The methods of Holloway *et al.* (2006), Bachu *et al.* (2007) (Table 3, equation 2) and Tseng *et al*. (2012) result in the same storage capacity estimates in each reservoir, and therefore show 0% difference in Figure 12.

Overall, the methods of Holloway *et al.* (2006), Bachu *et al.* (2007) (Table 3, equation 2) and Tseng *et al*. (2012) produce consistent, conservative estimates for CO_2 storage capacities in both the depletion drive and water drive reservoirs (see Fig. 12), and provide a good basis from which effective CO_2 storage capacities can be estimated.

All of the theoretical CO_2 storage capacity equations rely on either direct estimation of the OGIP, or the estimation of a parameter that relies upon the OGIP (such as the recovery factor), apart from the method of Tseng *et al*. (2012) (Table 3, equation 4). Therefore, it is important to obtain a precise value for the OGIP so that estimated CO_2 storage capacities are more accurate. This study has shown that aquifer modelling can help to avoid an overestimation of the OGIP in water drive reservoirs and give more accurate values of W_e to be input into storage capacity equations (i.e. positive values). However, there are alternative published methods, such as Bachu *et al*. (2007) (Table 3, equation 2) and Tseng *et al*. (2012), which do not require this level of detail. The theoretical method of Tseng *et al*. (2012)

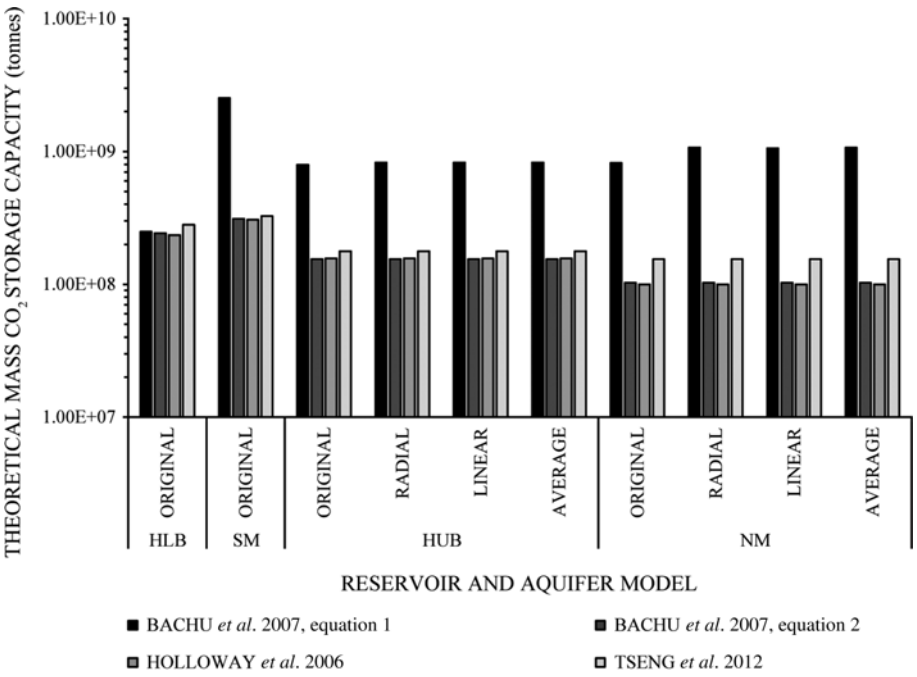

Fig. 11. Theoretical CO_2 storage capacity of the four reservoirs: Hewett Lower Bunter (HLB), South Morecambe (SM), Hewett Upper Bunter (HUB) and North Morecambe (NM). The capacities of all four reservoirs have been calculated using the originally estimated values for OGIP. The two water drive reservoirs (HUB and NM) also have estimates based on radial and linear aquifer modelling, and an average of the two models. Please note: results for the Hewett Upper Bunter Sandstone reservoir does not constitute an Eni interpretation or view.

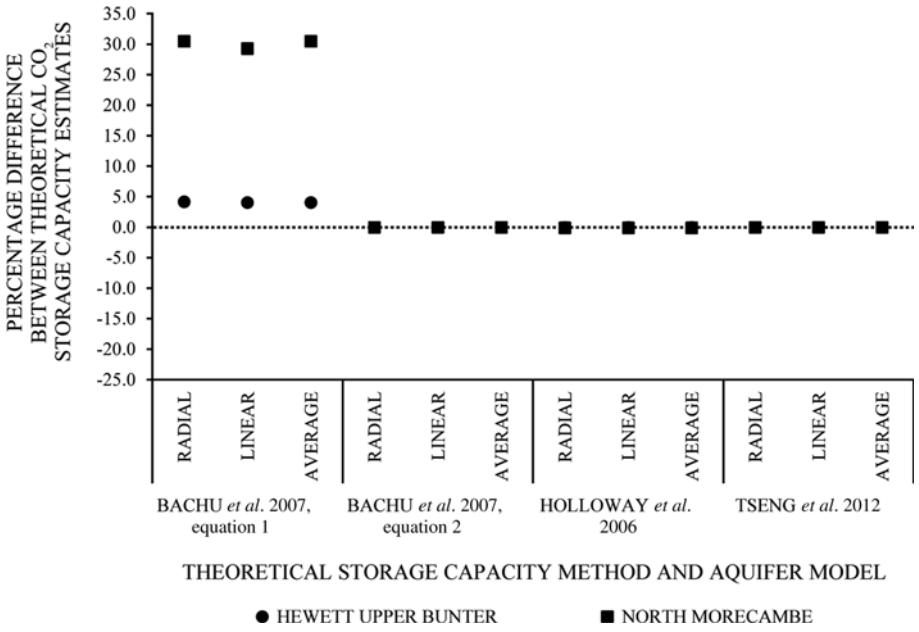

Fig. 12. Graph of percentage difference of theoretical CO_2 storage capacity estimates between estimates using the original OGIP values and revised OGIP estimates following aquifer modelling. The black dashed line indicates the baseline (i.e. no difference between estimates). Please note: results for the Hewett Upper Bunter Sandstone reservoir do not constitute an Eni interpretation or view.

completely avoids use of the OGIP or any dependent variables, and is not influenced by aquifer modelling since it avoids use of W_e (Fig. 12), whilst producing conservative, consistent capacity estimates (Fig. 11). The method of Bachu *et al.* (2007) (Table 3, equation 2) appears to give similar results despite it being possible to use incorrect OGIP values and dependent variables; as such, the method should be used with caution.

The geometric method of Bachu *et al.* (2007) (Table 3, equation 1) produces the greatest capacity estimates and is the method most susceptible to variability. The method is oversimplified as the gross reservoir volume is defined by only area and height: parameters that are difficult to quantify as individual values. The method can yield comparable results to the alternative theoretical methods in thin reservoirs (as is the case for the Hewett Lower Bunter Sandstone reservoir: see Fig. 11). However, in thicker reservoirs, it is assumed the whole thickness of the reservoir is entirely gas-bearing (particularly problematic in the Morecambe gas fields, which consist of illite-affected parts of the reservoir over a substantial thickness, and also with them being thick, dipping reservoirs mean that the gas-bearing volume is prism-shaped not box-shaped: Fig. 11). As such, it will always overestimate the true gross rock volume. A second issue with the method is that the cumulative volumes of injected and produced water are often not measured (as this is not necessary for successful production from gas reservoirs in most cases); therefore, any estimated values are likely to be incorrect. A final issue is the value used for water saturation: it is often assessed prior to production, but the value is likely to change as production progresses, particularly in water drive reservoirs, but is not often re-assessed.

The alternative theoretical methods of Holloway *et al.* (2006), Bachu *et al.* (2007) (Table 3, equation 2) and Tseng *et al.* (2012) generally predict comparable results and rely upon input parameters which can be well constrained, including initial pressures and temperatures within the gas reservoirs. However, this study has demonstrated that the values of parameters such as the OGIP, which is generally considered to be well constrained, should not necessarily be taken at face value. The Hewett Upper Bunter and North Morecambe reservoirs, originally modelled as depletion drive reservoirs, have original OGIP values that are overestimates. Therefore, it is imperative to ascertain whether a proposed storage reservoir experiences a water drive. If the OGIP is overestimated, it follows that the final theoretical CO_2 storage capacity estimates may be erroneous.

Figure 13 shows the effective CO_2 storage capacity results from all four reservoirs and these have been estimated using the method of Tseng *et al.* (2012) (Table 3, equation 5), based on the original OGIP estimates. The water drive reservoirs have additional results

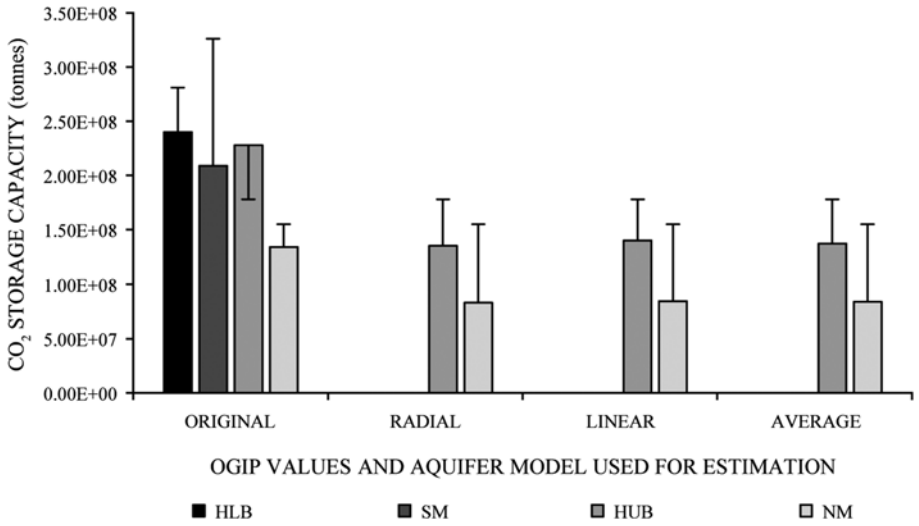

Fig. 13. Effective CO_2 storage capacity of the four reservoirs based on the method of Tseng *et al.* (2012): Hewett Lower Bunter (HLB), South Morecambe (SM), Hewett Upper Bunter (HUB) and North Morecambe (NM). The capacities of all four reservoirs have been calculated using the originally estimated values for OGIP. The two water drive reservoirs (HUB and NM) also have estimates based on radial and linear aquifer modelling, and an average of the two models. The bars represent the theoretical CO_2 storage capacity estimates using the theoretical method of Tseng *et al.* (2012). Please note: results for the Hewett reservoirs do not constitute an Eni interpretation or view.

from aquifer modelling. The bars in Figure 13 represent the theoretical CO_2 storage capacity estimates from the method of Tseng *et al.* (2012) (Table 3, equation 4). The effective capacity is, by definition, a subset (reduction) of the theoretical capacity and, in most cases here, the effective CO_2 storage capacity estimate is less than the corresponding theoretical estimate. The effective capacity of the Hewett Upper Bunter Sandstone reservoir based on the original OGIP values is greater than the theoretical capacity estimate and is further evidence that the original OGIP values are incorrect. Following aquifer modelling, the results from the water drive reservoirs seem more in line with expected results. In general, the effective capacities are between 64 and 86% of theoretical capacities within the depletion drive reservoirs, and are 53 – 79% within the water drive reservoirs.

The effective CO_2 storage capacity method of Tseng *et al.* (2012) (Table 3, equation 5 and 6) requires the cumulative volume of water influx into a reservoir, W_e, across the productive lifetime of a gas reservoir to be known. This parameter is especially sensitive to the estimated OGIP value; therefore, it is paramount this value is precise to obtain accurate effective CO_2 storage capacity estimates in water drive gas reservoirs. This can be achieved through aquifer modelling, as this study has shown. Within depletion drive reservoirs, the value of W_e will be zero or negligible. All other required parameters for this method are generally well constrained, including the cumulative volume of produced hydrocarbons which is constantly measured, being the saleable asset.

Conclusions

This study has shown that theoretical CO_2 storage capacity estimates vary as a result of several factors: (a) the reservoir drive mechanism (or degree of aquifer support a reservoir receives); (b) the method of storage capacity estimation used; and (c) the degree of natural variability of input parameters and/or overall accuracy of the input parameters.

The difficulties in solving the material balance equation in the presence of a water drive have been demonstrated here. Cole plots can provide a more definitive way of characterizing the reservoir drive mechanism as any deviation from a linear trend on the Cole plot denotes the presence of a water drive.

It is important to establish the correct reservoir drive mechanism so that more precise estimates of OGIP, and any dependent variables, can be input into theoretical and effective CO_2 storage capacity equations. Establishing a precise estimate of OGIP, on which the estimation of W_e relies, is of particular importance for effective CO_2 storage capacity estimation. Imprecise values can result in capacity being erroneously estimated. Aquifer modelling can be used to increase the precision of the OGIP estimates and their dependent variables; however, the resulting storage capacity estimate inevitably depends on the method being used.

The geometric theoretical CO_2 storage capacity method of Bachu *et al.* (2007) (Table 3, equation 1) consists of parameters which are oversimplistic for the treatment of individual gas fields and, as such, can result in considerable overestimates of CO_2 storage capacity. The alternative theoretical methods of Holloway *et al.* (2006), Bachu *et al.* (2007) (Table 3, equation 2) and Tseng *et al.* (2012) generally predict comparable results and rely on input parameters that can be well constrained with little variability. The theoretical method of Tseng *et al.* (2012) was found to give reliable estimates as it avoids input of the OGIP, or any dependent variables; however, aquifer modelling can be used to produce consistent, conservative theoretical CO_2 storage capacity results via the methods of Holloway *et al.* (2006) and Bachu et al. (2007).

Overall, theoretical CO_2 storage capacity estimates vary by 16% in the Hewett Lower Bunter reservoir, 81% in the Hewett Upper Bunter reservoir, 88% in the South Morecambe reservoir and 91% in the North Morecambe reservoir (percentage difference between the highest and lowest estimates, based on average aquifer models in the water drive reservoirs). Comparing the theoretical capacity estimates of Tseng *et al.* (2012) with the effective method of the same author, estimated effective capacities are between 64 and 86% of theoretical capacities within the depletion drive reservoirs, and 53 – 79% within the water drive reservoirs.

Acknowledgements

Our acknowledgements go to Eni Hewett Ltd, operator of the Hewett Unit assets, and their partner, Perenco UK (Gas) Ltd, for providing access to historical production and pressure data relating to the Hewett Unit gas fields. Our acknowledgements also go to Centrica, operator of the South and North Morecambe assets, for providing historical production and pressure data relating to the Morecambe gas fields. Please note that all interpretations made in the study, unless specifically stated, are those of the authors and do not necessarily reflect the views of Eni Hewett Ltd, Perenco UK (Gas) Ltd or Centrica. Similarly, previously published data used in the calculations and results for the Hewett reservoirs do not constitute an Eni Hewett Ltd interpretation or view. ALC would like to take this opportunity to thank her CASE partners, IHS and Badley Geoscience Ltd, for the provision of data, training and guidance during her research on the Hewett and Morecambe gas fields.

Funding ALC would like to acknowledge funding by NERC (NERC Open CASE studentship to Durham University, grant reference NE/G011222/1). JI is part-funded by the Royal Society (Royal Society Industry Fellowship with Badley Geoscience Ltd and Geospatial Research Ltd).

References

Agarwal, R.G., Al-Hussainy, R. & Ramey H. J., Jr. 1965. The importance of water influx in gas reservoirs. *Journal of Petroleum Technology*, **17**, 1336–1342.

Archer, J.S. & Wall, C.G. 1986. *Petroleum Engineering: Principles and Practice*. Graham & Trotman, London.

Bachu, S., Bonijoly, D., Bradshaw, J., Burruss, R., Holloway, S., Christensen, N.P. & Mathiassen, O.M. 2007. CO_2 storage capacity estimation: Methodology and gaps. *International Journal of Greenhouse Gas Control*, **1**, 430–443.

Bastin, J.C., Boycott-Brown, T., Sims, A. & Woodhouse, R. 2003. The South Morecambe Gas Field, Blocks 110/2a, 110/3a, 110/7a and 110/8a, East Irish Sea. *In*: Gluyas, J.G. & Hichens, H.M. (eds) *United Kingdom Oil and Gas Fields Commemorative Millennium Volume*. Geological Society, London, Memoirs, **20**, 107–118, https://doi.org/10.1144/gsl.mem.2003.020.01.09

Bentham, M. 2006. *An Assessment of Carbon Sequestration Potential in the UK – Southern North Sea Case Study*. Tyndall Centre Working Paper 85. Tyndall Centre for Climate Change Research.

Brook, M., Shaw, K., Vincent, C. & Holloway, S. 2003. *Gestco Case Study 2a-1: Storage Potential of the Bunter Sandstone in the UK sector of the Southern North Sea and the Adjacent Onshore Area of Eastern England*. BGS Commissioned Report CR/03/154N. British Geological Survey, Keyworth, Nottingham.

Bruns, J.R., Fetkovich, M.J. & Meitzen, V.C. 1965. The effect of water influx on P/z-cumulative gas production curves. *Journal of Petroleum Technology*, **17**, 287–291.

Chierici, G.L., Pizzi, G. & Ciucci, G.M. 1967. Water drive gas reservoirs: uncertainty in reserves from past history. *Journal of Petroleum Technology*, **19**, 237–244.

Clarke, A., Imber, J. *et al*. 2010. Hewett: a promising carbon storage site? Paper presented at the *Petroleum Geoscience Research Collaboration Showcase*, 23–24 November 2010, London.

Cole, F.W. 1969. *Reservoir Engineering Manual*. Gulf Publishing, Houston, TX.

Cooke-Yarborough, P. & Smith, E. 2003. The Hewett Fields: Blocks 48/28a, 48/29, 48/30, 52/4a, 52/5a, UK North Sea: Hewett, Deborah, Big Dotty, Little Dotty, Della, Dawn and Delilah Fields. *In*: Gluyas, J.G. & Hichens, H.M. (eds) *United Kingdom Oil and Gas Fields Commemorative Millennium Volume*. Geological Society, London, Memoirs, **20**, 731–739, https://doi.org/10.1144/gsl.mem.2003.020.01.60

Cowan, G. & Boycott-Brown, T. 2003. The North Morecambe Field, Block 110/2a, East Irish Sea. *In*: Gluyas, J.G. & Hichens, H.M. (eds) *United Kingdom Oil and Gas Fields Commemorative Millennium Volume*. Geological Society,

London, Memoirs, **20**, 97–105, https://doi.org/10.1144/gsl.mem.2003.020.01.08

Dake, L.P. 1978. *Fundamentals of Reservoir Engineering*. Elsevier Scientific, Amsterdam.

Global CCS Institute. 2015. *The Global Status of CCS 2015*. Global CCS Institute, Melbourne, Australia.

Hagoort, J. 1988. Chapter 11: Natural depletion. *In:* Hagoort, J. (ed.) *Developments in Petroleum Science*. Elsevier Science, New York, 233–261, https://doi.org/10.1016/s0376-7361(09)70333-4

Holloway, S. 2009. Storage capacity and containment issues for carbon dioxide capture and geological storage on the UK continental shelf. *Proceedings of the Institution of Mechanical Engineers, Part A: Journal of Power and Energy*, **223**, 239–248.

Holloway, S., Vincent, C.J. & Kirk, K.L. 2006. *Industrial Carbon Dioxide Emissions and Carbon Dioxide Storage Potential in the UK*. British Geological Survey, Keyworth, Nottingham.

Jackson, D.I., Jackson, A.A., Evans, D., Wingfield, R.T.R., Barnes, R.P. & Arthur, M.J. 1995. *The Geology of the Irish Sea*. British Geological Survey, United Kingdom Offshore Regional Report Series. British Geological Survey, Keyworth, Nottingham.

Johnson, H., Warrington, G. & Stoker, S.J. 1994. 6. Permian and Triassic of the Southern North Sea. *In*: Knox, R.W.O. & Cordey, W.G. (eds) *Lithostratigraphic Nomenclature of the UK North Sea*. British Geological Survey, Keyworth, Nottingham.

Kirk, K.L. 2006. *Potential for Storage of Carbon Dioxide in the Rocks Beneath the East Irish Sea*. British Geological Survey, Keyworth, Nottingham.

Lemmon, E.W., Huber, M.L. & McLinden, M.O. 2013. *NIST Standard Reference Database 23: Reference Fluid Thermodynamic and Transport Properties – REFPROP.* National Institute of Standards and Technology (NIST), Gaithersburg, MD.

Payne, D.A. 1996. Material-balance calculations in tight-gas reservoirs: The pitfalls of p/z plots and a more accurate technique. *SPE Reservoir Engineering*, **11**, 260–267.

Peng, D.-Y. & Robinson, D.B. 1976. A new two-constant equation of state. *Industrial & Engineering Chemistry Fundamentals*, **15**, 59–64, https://doi.org/10.1021/i160057a011

Pletcher, J.L. 2002. Improvements to reservoir material-balance methods. *SPE Reservoir Evaluation & Engineering*, **5**, 49–59.

Stuart, I.A. 1993. The geology of the North Morecambe Gas Field, East Irish Sea Basin. *In*: Parker, J.R (ed.) *Petroleum Geology of Northwest Europe: Proceedings of the 4th Conference*. Geological Society, London, Petroleum Geology Conference Series, **4**, 883–895, https://doi.org/10.1144/0040883

Stuart, I.A. & Cowan, G. 1991. The South Morecambe Field, Blocks 110/2a, 110/3a, 110/8a, UK East Irish Sea. *In*: Abbotts, I.L. (ed.) *United Kingdom Oil and Gas Fields, 25 Years Commemorative Volume*. Geological Society, London, Memoirs, **14**, 527–541, https://doi.org/10.1144/gsl.mem.1991.014.01.66

Tseng, C.-C., Hsieh, B.-Z., Hu, S.-T. & Lin, Z.-S. 2012. Analytical approach for estimating CO_2 storage capacity of produced gas reservoirs with or without a water drive. *International Journal of Greenhouse Gas Control*, **9**, 254–261, https://doi.org10.1016/j.ijggc.2012.04.002

Van Everdingen, A.F. & Hurst, W. 1949. The application of the Laplace transformation to flow problems in reservoirs. *Journal of Petroleum Technology*, **1**, 305–324.

Vega, L. & Wattenbarger, R.A. 2000. New approach for simultaneous determination of the OGIP and aquifer performance with no prior knowledge of aquifer properties and geometry. Paper presented at the *SPE/CERI Gas Technology Symposium*, 3–5 April 2000, Calgary, Alberta, Canada.

Wang, B. & Teasdale, T.S. 1987. GASWAT-PC: A microcomputer program for gas material balance with water influx. Paper presented at the *Petroleum Industry Application of Microcomputers Conference*, 23–26 June 1987, Lake Conroe, Texas.

Warrington, G., Audley-Charles, M.G. *et al*. 1980. *A Correlation of Triassic Rocks in the British Isles*. Geological Society, London, Special Reports, **13**.

Wibberley, C.A.J. 2002. Hydraulic diffusivity of fault gouge zones and implications for thermal pressurisation during seismic slip. *Earth, Planets and Space*, **54**, 1153–1171.